Yang Li, Peng Xiao, Heng Luo, Renato S. M. Almeida, Zhuan Li, Wei Zhou, Alexander Brückner, Florian Reichert, Nico Langhof, Walter Krenkel

# Fatigue behavior and residual strength evolution of 2.5D C/C-SiC composites



Yang Li, Peng Xiao, Heng Luo, Renato S.M. Almeida, Zhuan Li, Wei Zhou, Alexander Brückner, Florian Reichert, Nico Langhof, Walter Krenkel,
Fatigue behavior and residual strength evolution of 2.5D C/C-SiC composites,
Journal of the European Ceramic Society, Volume 36, Issue 16, 2016, Pages 3977-3985, ISSN 0955-2219,
https://doi.org/10.1016/j.jeurceramsoc.2016.07.009

# Fatigue behavior and residual strength evolution of 2.5D C/C-SiC composites

Yang Li[a,b], Peng Xiao[a,*], Heng Luo[a], Renato S.M. Almeida[c], Zhuan Li[a,*], Wei Zhou[a], Alexander Brückner[d], Florian Reichert[b], Nico Langhof[b], Walter Krenkel[b]

[a] State Key Laboratory of Powder Metallurgy, Central South University, Changsha 410083, PR China
[b] Ceramic Materials Engineering, University of Bayreuth, Bayreuth, 95447, Germany
[c] Advanced Ceramics, University of Bremen, Bremen, 28359, Germany
[d] Polymer Engineering, University of Bayreuth, Bayreuth, 95447, Germany

*Keywords:*
C/C-SiC
Tensile fatigue
Mechanical evolution
Residual strength

A B S T R A C T

The residual tensile strength (RTS) evolution of a chemical vapor infiltration and liquid silicon infiltration based 2.5 dimensional reinforced C/C-SiC (2.5D C/C-SiC) composites after fatigue loadings has been investigated. The results show that the fatigue limit ($10^6$ cycles) of the 2.5D C/C-SiC composites reaches 58.2 MPa, which corresponds to 75% of the virgin static tensile strength (77.7 MPa). Moreover, an ultimate strength enhancement is observed after fatigue loading. The most pronounced RTS increases to 92.5 MPa when specimens are subjected to fatigue stress of 69.3 MPa for $10^5$ cycles. The microstructural analysis indicates that RTS after cyclic loading is affected by the formation and propagation of cracks and interfacial degradation. Furthermore, a model proposed in this work can well evaluate the RTS of the composites in relation to the number of the applied fatigue cycles.



## 1. Introduction

Ceramic matrix composites (CMCs) show high strength with considerable fracture toughness, and are initially developed for aeronautical purposes [1,2]. Nowadays, the related processing methods have reached a high level of reproduction, and since the 1990s, the liquid silicon infiltration (LSI) method has allowed the production of C/C-SiC composites with relatively low costs [3,4]. Therefore, their areas of application have been widened to industrial applications like ceramic brake discs for sports cars and luxury sedans [5]. In this context, the needled carbon fabric preforms are promising candidates for the production of 2.5 dimensional C/C-SiC composites (2.5D C/C-SiC). These composites show excellent mechanical properties, good coefficient of friction, relatively low manufacture cost and excellent humidity tolerance in tribological applications [6]. Hence, the 2.5D C/C-SiC composites present enormous potential applications in high-speed and heavy-duty brake systems [6–8]. Currently, most works regarding the 2.5D C/C-SiC materials are focused on the topics of cost reduction, mechanical optimization, friction behaviors and even industrial applications for service and emergency brake in the trains or aircrafts [9–14]. However, there are still few investigations concentrating on the influence of dynamic loadings on the long-term mechanical performances of these 2.5D C/C-SiC composites. It is generally believed that the cyclic stresses during practical service can lead to the degradation of strength and even catastrophic failures in CMCs [15–18]. Thus, it is of great significance to get a comprehensive investigation on the mechanical behaviors of the 2.5D C/C-SiC composites under dynamic loads. Therefore, this work aims to study the fatigue behavior and the evolution of residual tensile strength (RTS) of the 2.5D C/C-SiC composites subjected to different fatigue loadings. Experimentally, the fatigue behavior including the stress versus cycles to failure (S-N curves), RTS after preselected cyclic loadings were investigated. Moreover, the microstructures and fractured surfaces were characterized by optical microscope (OM) and scanning electron microscope (SEM) to study the fatigue damage behavior. Finally, a mechanical model was introduced, based on the experimental results, to describe the RTS evolution of the 2.5D C/C-SiC composites in relation to the number of fatigue cycles.

* Corresponding authors.
*E-mail addresses:* xiaopeng@csu.edu.cn (P. Xiao), lizhuan@csu.edu.cn (Z. Li).

## 2. Materials and experiments

### 2.1. Fabrication of the composites

The fabrication process of 2.5D C/C-SiC composites consisted of the following three steps as shown in Fig. 1. The commercially available polyacrylonitrile (PAN) based carbon fiber (Toray, Japan, T700, 12k) were applied as raw material for the 2.5D fiber preforms. Firstly, the short fiber web and the unidirectional fiber cloth were repeatedly stacked and afterwards needle-punched. The needle punching density was 15–35 pin $cm^{-2}$ and the bulk density of the 2.5D fiber preform was approximately 0.65 g $cm^{-3}$. Afterwards, the chemical vapor infiltration (CVI) process at 1000 °C for 100–120 h in an argon atmosphere with the absolute pressure of 0.1 MPa was performed. The $C_3H_6$ was applied as a precursor and $H_2$ as a carrier and diluting gas ($C_3H_6/H_2$ = 10 ml $min^{-1}$: $H_2$ = 20 ml $min^{-1}$). The final step was the preparation of the C/C-SiC by an infiltration of liquid silicon (LSI) into the porous C/C material. The silicon powders (Da Zelin-silicon Co., LTD, Beijing, China) with the particle size of approximately 50 μm and a purity of 99.0% were applied for LSI, and the process was carried out at 1650 °C with 0.5 h dwell time under vacuum conditions (absolute pressure <1 Pa). More details about the fabrication process of the 2.5D C/C-SiC was reported previously [7].

### 2.2. Initial characterization

The initial characterizations were done concerning the porosity, bulk density and virgin tensile strength. Therefore, all specimens were machined to obtain a grinded and polished surface. The open porosity and the bulk density of the as-processed 2.5D C/C-SiC composites were measured by the Archimedes method with distilled water, following the standard DIN EN 1389. The dog-bone shaped specimens for the tensile tests were prepared by wire eroding with the general dimensions, which can be seen in Fig. 2. In order to avoid grip slipping during the tensile loading, the clamped portions of the specimens were coated by a cured adhesive (allcon10 original, Beko, Germany) with a thickness of about 0.75 mm. Quasi-static tensile tests were performed on a Zwick/Roell test machine (Z1485, Makro, 250 kN) with a crosshead speed of 1 mm/min, following the standard DIN EN 658-1.

### 2.3. Tensile fatigue tests

According to the standard ASTM C1360, the tensile-tensile fatigue experiments were performed following a sinusoidal wave with the frequency of 10 Hz and the fatigue stress ratio of 0.1 on a servo hydraulic testing machine (IST Hydro pulse MHF). In this work, three sets of cyclic loadings were performed on the specimens to study the fatigue behaviors. Initially, within the “Set 1”, the specimens were tested with five different stresses (75%, 80%, 85%, 90% and 95% of the initial tensile strength, corresponding to about 58.2, 62.1, 66, 69.3 and 73.8 MPa, respectively) to define the fatigue limit. The specimens were cyclically loaded until total failure or until run-out, defined here as $10^6$ cycles, was reached. During the tests, a period of approximately 1000 cycles was required to achieve the desired maximum stress.

Afterwards, the fatigue tests were performed to analyze the stress dependence of RTS within the “Set 2”. To ensure that the samples would not fail during the fatigue tests, the run-out was reduced to $10^5$ cycles. For these tests, four stress levels ranging from 75% to 90% were applied. In addition, within “Set 3”, fatigue cycles with different numbers of pre-selected cycles ($10^4$, $10^5$ and $10^6$, respectively) were performed at the stress level of 75% (58.2 MPa). Three sets of tests were performed in a strain-control mode with the parameters shown in Table 1. Quasi-static tensile tests were then carried out, following the aforementioned procedure, in order to measure the RTS after fatigue loadings.

Finally, the microstructure, the fractured surfaces and the type of fracture were studied by an optical microscope (Axiotech HAL100, Zeiss) and a scanning electron microscope (SEM, FEI Nova Nano SEM-230).

## 3. Results and discussion

### 3.1. Fatigue life time of the 2.5D C/C-SiC composites at room temperature

The general properties of the as-processed 2.5D C/C-SiC composites before fatigue test are summarized in Table 2. The 2.5D C/C-SiC composites are dense and show a mean tensile strength of 77.7 MPa after the quasi-static tensile tests.

Fig. 3 presents the diagram of stress versus cycles to failure (S-N curve) for the 2.5D C/C-SiC composites at room temperature. The failure of the cyclic loaded specimens depends on the applied stress level. As shown in Fig. 3, all specimens subjected to the stresses which are higher than 80% of the static tensile strength failed before finishing the test. When the stress level is 80%, only one-third of the tested specimens failed before achieving the desired $10^6$ cycles. However, when the stress level decreases to 75%, all of the three specimens could undertake the fatigue loading for $10^6$ cycles. Hence, the 2.5D C/C-SiC composites exhibit a high resistance to the fatigue stress and the fatigue limit ($10^6$ cycles) is probably around 58.2 MPa, corresponding to 75% of the virgin tensile strength.

### 3.2. Stress-dependence of the residual tensile strength

The dynamic modulus (DM) versus fatigue cycles with the fatigue stress levels of 75% and 90% is shown in Fig. 4(a). During the cyclic loading, an initial decrease of the DM was observed. This decrease can be related to the rapid initiation and the growth of matrix cracks. The effect of matrix cracks deflecting around the fibers should also be taken into account as it leads to relative movements between fiber/matrix. Subsequently, the DM are roughly stabilized, which indicates that almost no new formation of cracks occured (near saturation of cracks). Moreover, it is found that the higher applied fatigue stress leads to more fatigue damages and results in a relatively lower DM. In addition, the DM fluctuates slightly due to the opening-closing effects of cracks under cyclic loading.

Fig. 4(b) shows the relationship of the RTS/elastic modulus versus four different stress levels. For the same reason discussed above, the fatigue loadings lead to reductions for the measured elastic modulus. The similar phenomena were also observed in other CMCs [19,20]. However, no significant difference is observed between different fatigue stress levels. This can be explained by the “self-healing” effect of the composite. During unloading, the formed cracks are partially closed, and the matrix cracks/fibers tend to move to their original places. This can also explain why the DM behaves differently than the resultant E-modulus. In contrast to the decreasing modulus, the samples which were previously loaded with different stresses for $10^5$ cycles consistently show an increase of residual tensile strength (RTS). The RTS incline to increase with the higher stress levels. Compared to the virgin samples (about 77.7 MPa), the RTS after the fatigue loadings with the stress levels of 75%, 80%, 85% and 90% for $10^5$ cycles increase to $85.8 \pm 16.3$, $84.3 \pm 17.3$, $86.6 \pm 5.8$ and $92.5 \pm 8.3$ MPa, respectively. This enhancement of the composite strength can be mainly explained in matters of reduction of internal stresses due to matrix cracking and interfacial degradation, which are also consistent with the other composites as reported in previous studies [21,22].

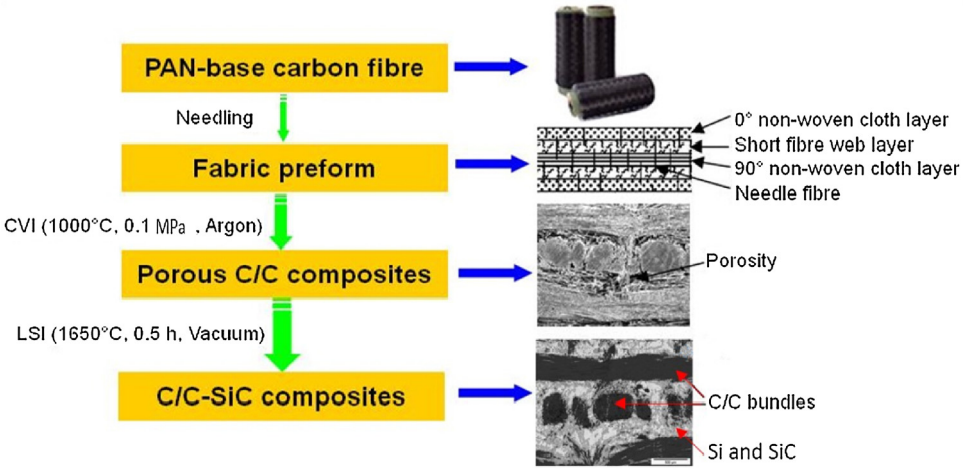


**Fig. 1.** Schematic illustration of the manufacturing process for the 2.5D C/C-SiC composites.

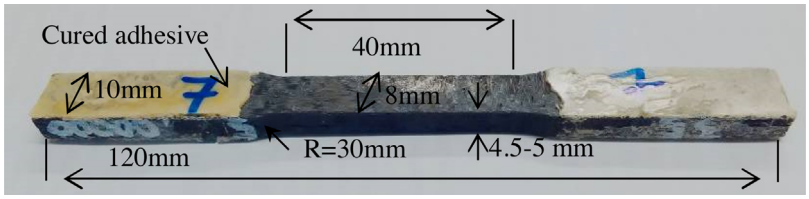


**Fig. 2.** Photograph of the tensile specimens.

**Table 1**
The preselected parameters for fatigue tests of 2.5D C/C-SiC composites.

| Experimental serial No. | Fatigue cycles | Fatigue stresses and the corresponding fatigue stress levels | | | | |
|---|---|---|---|---|---|---|
| "Set 1" | $\leq 10^6$ | 58.2 MPa, 75% | 62.1 MPa, 80% | 66 MPa, 85% | 69.3 MPa, 90% | 73.8 MPa, 95% |
| "Set 2" | $10^5$ | 58.2 MPa, 75% | 62.1 MPa, 80% | 66 MPa, 85% | 69.3 MPa, 90% | |
| "Set 3" | $10^4$ | 58.2 MPa, 75% | | | | |
| | $10^5$ | 58.2 MPa, 75% | | | | |
| | $10^6$ | 58.2 MPa, 75% | | | | |

**Table 2**
The general properties of the as-processed 2.5D C/C-SiC composites.

| Sample | Fiber volume fraction | Bulk density/g cm$^{-3}$ | Open porosity/% | Tensile strength (MPa) | Failure strain (%) | Elastic modulus (GPa) | Number of tested sample |
|---|---|---|---|---|---|---|---|
| C/C-SiC | 30–35% | 2.1 (0.1) | 4.5 (0.5) | 77.7 (15.6) | 0.37 (0.05) | 34.5 (7.7) | N = 7 |

Standard deviations are given in parentheses.

The mechanical behavior of the composite after fatigue loadings is also analyzed. Fig. 4(c) presents the representative tensile stress-strain curves of original and fatigue loaded samples with stress levels of 80% and 90% for $10^5$ cycles. In order to enhance the readability of the figure, the starting point in the stress-strain curve for the fatigue loaded sample (previously loaded with stress level of 90% for $10^5$ cycles) is artificially shifted to a strain of 0.1%. The stress-strain curve of the virgin sample shows a linear-elastic behavior followed by a substantially extent of a non-linear region. As for the CMCs, such phenomenon is normally derived from a variety of modes associated with matrix cracking and later fiber damage in composites [23,24]. Initially, when the applied tensile stress is low, the process-induced cracks in the virgin sample do not propagate, showing a transient linear behavior. However, as the load gradually increases, cracks arise and/or propagate in the matrix. As the load increases continuously, the matrix cracking reaches a certain level, at which the matrix can not support the applied load, and most of the loads are transferred to the fibers. This leads to the uncorrelated rupture of the fibers, which results in non-linear elastic behavior and a decreasing tangent modulus observed in the stress-strain curve.

By contrast, the typical stress-strain curves of fatigued 2.5D C/C-SiC specimens as displayed in Fig. 4(c) shows nearly only linear elastic behaviors when the applied tensile stresses are lower than previous fatigue stresses. In other words, non-linearity is only observed after reaching the previously applied fatigue stress. This goes well with the fact that cracks already appeared and propagated during fatigue. Hence, new damage is only detectable and the cracks are activated in the composites if the applied tensile stress is higher than previous fatigue stress. Generally, the tensile behavior of the fatigued samples shows a dependence on the maximum

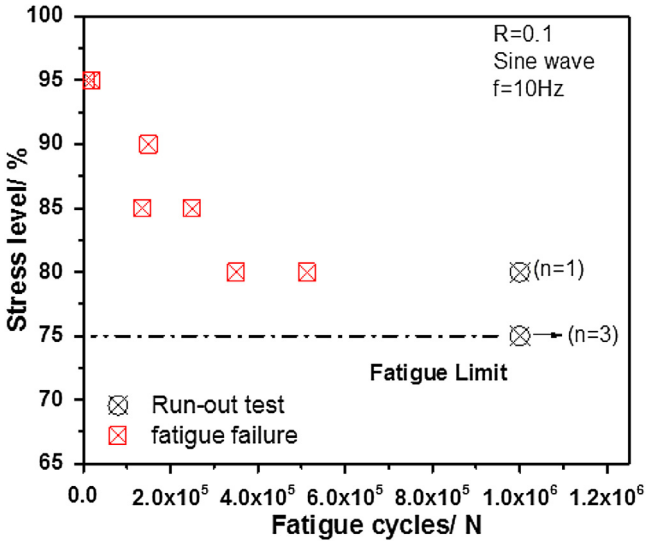


**Fig. 3.** The diagram of stress versus cycles to failure (S-N curve) for the 2.5D C/C-SiC composites at room temperature. The horizontal arrows indicate the samples that achieved the run-out of $10^6$ cycles, n in the bracket refers to the number of valid samples.

applied fatigue stress. This so called stress-memory effect was also observed in the Refs. [22,24].

### 3.3. *Cycle-dependence of the residual tensile strength*

It is known that the RTS and fatigue behavior of CMCs are not only dependent on the applied fatigue stress but also closely related to the fatigue cycles [20,21]. Hence, the specimens are also tested with the stress level of 75% (about 58.2 MPa) for $10^4$, $10^5$ and $10^6$ cycles in this study. To analyze the fatigue behavior, Fig. 5(a) shows 5 stress-strain loops recorded at 14, 111,070, 435,350, 888,800 and 999,950 cycles. It is clear that the hysteresis loop area (HLA) observed in the beginning, 14th cycle, is smaller than the one at 111070th cycle. This is because the maximum fatigue stress had not yet reached a,fter merely 14 cycles. When the fatigue stress is stabilized to 58.2 MPa, the HLAs observed in the range from 111,070th cycle to 999,950th cycle are roughly the same. Furthermore, the hysteresis loops start to overlap and the permanent strains are almost constant after 435,350 cycles. This also demonstrates that the cracking in the composites is probably saturated.

Fig. 5(b) shows the typical stress-strain curves of virgin and fatigue loaded samples after the preselected fatigue cycles. In order to enhance the readability of the figure, the starting points in the stress-strain curves for the virgin sample and the sample, fatigue loaded for $10^4$ cycles, are artificially shifted to the strains of 0.1% and 0.025%, respectively. Compared to the curve of the virgin specimen, all fatigue loaded samples with a fatigue stress of 58.2 MPa (corresponding to the stress level of 75%) for different cycles display very similar linear behavior until the stress limit is reached in the static tensile test. Note that the linear behavior is independent on the above-mentioned fatigue cycles, and the sample loaded for $10^6$ cycles shows almost the same linearity as the sample loaded for $10^4$ cycles. Furthermore, the static tensile results of the virgin and fatigue loaded specimens after preselected cycles are summarized in Table 3.

As listed in Table 3, the previous fatigue stresses reduce the elastic modulus of the fatigue loaded specimens. Nevertheless, the RTS of the fatigued specimens increase after $10^4$ and $10^5$ cycles, and then decrease after $10^6$ cycles. At first, the notable increase of RTS of the fatigue loaded specimens confirms the existence of strength enhancement behavior induced by fatigue loading. However, as

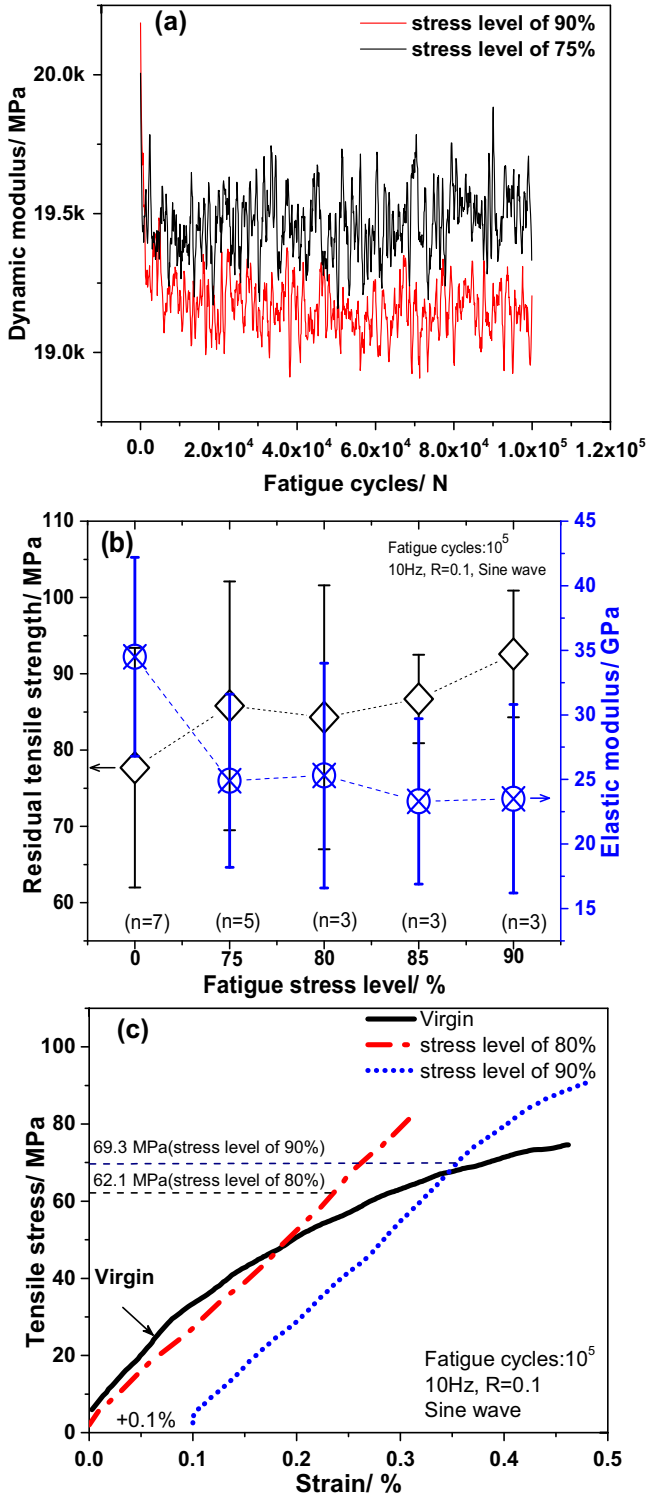


**Fig. 4.** (a) Dynamic modulus (DM) versus cycles under 75% and 90% of tensile stress; (b) Effect of the stress level on the retained strength and elastic modulus; (c) The typical tensile stress-strain curves of 2.5D C/C-SiC composites before and after $10^5$ cycles with 2 stress levels (80% and 90%). n in the bracket indicates the number of tested samples.

the fatigue cycles increase, the increment of RTS become less pronounced and the RTS reduces from the peak value of 85.8 MPa after $10^5$ cycles to 82.8 MPa after $10^6$ fatigue cycles. Predictably, the RTS of the 2.5D C/C-SiC will further decrease with more applied cycles. Thus, one can conclude that the proper fatigue loading could enhance the strength of the 2.5D C/C-SiC composites, with

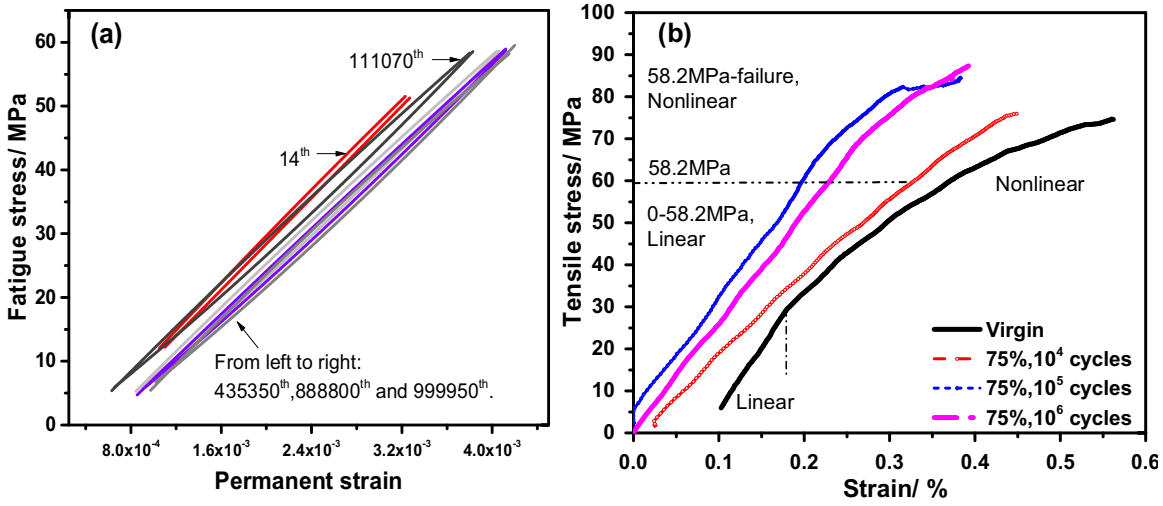


**Fig. 5.** (a) Stress-strain hysteresis loops with stress level of 75%. (b) The typical tensile stress-strain curves of 2.5D C/C-SiC composites after different fatigue cycles with the stress level of 75%.

**Table 3**
Static tensile test result of 2.5D C/C-SiC composites after the preselected fatigue cycles.

| Sample | Fatigue cycles | Fatigue stress/MPa | Static tensile strength/MPa | Failure strain/% | Elastic modulus/GPa | Number of tested sample |
|---|---|---|---|---|---|---|
| Virgin | No | no | 77.7 (15.7) | 0.37 (0.05) | 34.5 (7.7) | N = 7 |
| Fatigued | $10^4$ | 58.2 | 79.7 (10.1) | 0.41 (0.05) | 24.4 (5.3) | N = 5 |
| Fatigued | $10^5$ | 58.2 | 85.8 (16.3) | 0.41 (0.05) | 24.9 (6.7) | N = 5 |
| Fatigued | $10^6$ | 58.2 | 82.8 (6.4) | 0.36 (0.04) | 24.2 (2.7) | N = 4 |

Standard deviations are given in parentheses.

the expense of its non-linear behavior. Nevertheless, the excessive fatigue with overloading or too long time will be undoubtedly detrimental to the strength.

### 3.4. Microstructures

It is generally known that the fatigue loading could influence the evolution of defects in the composite. Therefore, optical microscopic observations were performed in order to characterize the distribution of the defects on specimens as-produced and after fatigue loadings. As shown in Fig. 6(a), the virgin sample already has several transverse cracks, marked with red arrows, distributed between the needled bundles. Moreover, longitudinal cracks, marked with blue arrows, and randomly oriented cracks, marked with yellow arrows, are also observed, but are comparatively less and shorter in comparison to the transverse cracks.

Theoretically, the mismatch of the coefficients of thermal expansion (CTE), of the different components, will result in thermal residual stresses (TRS) in the as-produced 2.5D C/C-SiC specimens, as shown in Fig. 7. The TRS in the composites consists of the tensile stresses within the transverse fiber cloth (0° fiber), the compressive stresses within the longitudinal fiber cloth (90° fiber) and the combination of compressive-compressive stresses in the fiber-needled region. In this sense, it is generally known that the TRS in CMC is directly related to the matrix cracking [22]. More specifically, TRS is responsible for the observed transverse cracks.

Fig. 6(b–d) shows the typical optical microstructures of the 2.5D C/C-SiC after fatigue loading for $10^4$, $10^5$ and $10^6$ cycles, respectively. It can be perceived that the fatigue stresses induce new transversely matrix cracks in the short fiber web layer and 0° fiber cloth, and enable the initial cracks to fully propagate at the same time. More cracks, which are connected with each other, were observed after more fatigue cycles applied. It is noteworthy that amount of both longitudinal and randomly oriented cracks increase after fatigue loading. Moreover, most of the longitudinal cracks were observed in boundary areas between the 0° fiber cloth and short fiber web layer. The different load-carrying capacities of 0° fiber cloth and short fiber layers result in different deformations, which gradually make these fiber layers detaching during the fatigue test. By contrast, the randomly oriented cracks tend to initiate near to the needle fiber bundles. The orientation of these cracks is determined by the combined effect of the TRS and applied fatigue load.

Fig. 8 shows the SEM micrograph of the fractured morphology of the 2.5D C/C-SiC composites. The matrix cracking in chopped fiber web and 0° fiber cloth could be observed after the static tensile test, as shown in Fig. 8(a). Additionally, the cracks-deflection occurs when the cracks propagate in the matrix.

Fig. 8(b)–(d) presents the fractured surfaces of the original specimens, the fatigue loaded specimens with the stress of 69.9 MPa for $10^5$ cycles and the fatigue loaded specimens with the stress of 58.2 MPa for $10^6$ cycles after static tensile tests, respectively. Different morphologies of the pull-out fiber clusters in virgin and fatigue loaded specimens are evidently presented. As shown in Fig. 8(b), the pull-out of fibers is mainly composed of clustered fibers and few single fibers in the virgin specimen. In addition, fragments of matrix in these clusters can be observed. Nevertheless, the fiber pull-out patterns shown in Fig. 8(c) and (d) mainly consist of single fibers and small fiber bundles. Generally, more pull-out of single fiber and small bundles indicate a further interfacial degradation.

In summary, the damage development during fatigue loading plays an important role in the mechanical behavior afterwards. The cracks multiplication relieves the TRS described in Fig. 7. After the removal of the TRS in the composites, more fiber bundles enable to carry the applied load uniformly and simultaneously. In a first moment, there is an increase of the RTS. These cracks concentrate

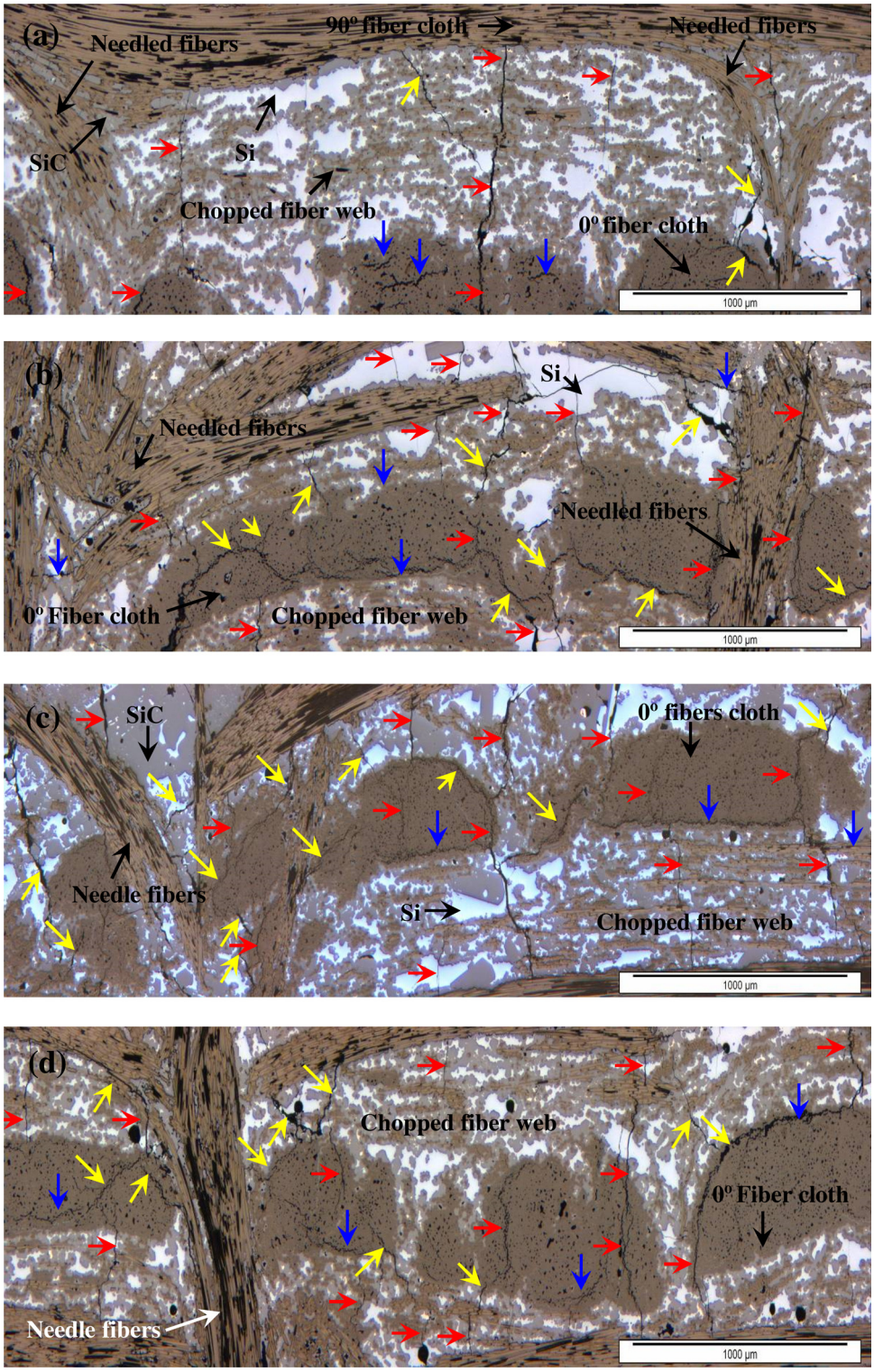


**Fig. 6.** Typical microstructures of 2.5D C/C-SiC before/after fatigue loading. (a) Virgin specimen without fatigue loading; (b) Specimen after fatigue with stress level 75% for $10^4$ cycles; (c) Specimen after fatigue with stress level 75% for $10^5$ cycles; (d) Specimen after fatigue with stress level 75% for $10^6$ cycles. The images show transverse cracks (red arrows) and longitudinal cracks (blue arrows) and randomly oriented cracks (yellow arrows). Fatigue loading was along with the 90° fiber orientation. (For interpretation of the references to colour in this figure legend, the reader is referred to the web version of this article.)

between the border of different fiber orientations, and in the needled fibers. As the number of cycles increase, these cracks promote the detachment and relative movement of the short fibers. This has a direct influence over the post fracture mechanism, as seen in Fig. 8. If more fatigue cycles are applied, the interfacial sliding of the fibers will result in interfacial debonding or even fiber wear. Therefore, the fatigue loading for a long period will change the interfacial sliding resistance and introduce new flaws into the fibers, which in turn will reduce the RTS [21,25].

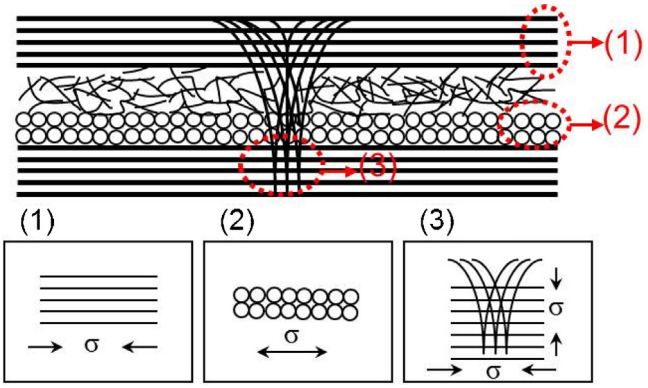


**Fig. 7.** Schematic sketch of three kinds of thermal residual stresses in 2.5D C/C-SiC composites.

### 3.5. Residual strength model for 2.5D C/C-SiC composites

It is generally believed that the RTS decreases with the increasing fatigue cycles. However, as aforementioned, the RTS of the 2.5D C/C-SiC composites firstly increases until a maximum of 85.8 MPa after $10^5$ cycles, to then decreases slightly to 82.8 MPa after $10^6$ cycles. A similar behavior could also be found for other CMCs [19,22]. For a detailed investigation of this notable fatigue behavior of the 2.5D C/C-SiC composites, herein the RTS in this work can be divided into three parts, based on [26–28]:

$$\sigma_{residual} = \sigma_s + \Delta\sigma_{FR} + \Delta\sigma_{FD} \quad (1)$$

$$\Delta\sigma_{FR} = \sigma^c_{\max}\left[1 - e^{\left(\frac{-n}{N_{FR}}\right)}\right] \quad (2)$$

$$\Delta\sigma_{FD} = \sigma^c_{\max}\left[1 - e^{\left(\frac{n}{N_{FD}}\right)}\right] \quad (3)$$

Where $\sigma_{residual}$ is the RTS after $n$ cycles with the applied fatigue stress $\sigma_{\max}$, $\sigma_s$ is the initial quasi-static tensile strength, $\Delta\sigma_{FR}$ is fatigue-induced strength enhancement, $\Delta\sigma_{FD}$ is fatigue-induced strength degradation, $c$ is a constant, which is dependent on the fatigue stress and material type. $N_{FR}$ is the number of fatigue cycles before which the fatigue-induced reinforcement dominates. $N_{FD}$ is the number of fatigue cycles after which the fatigue-induced degradation occurs.

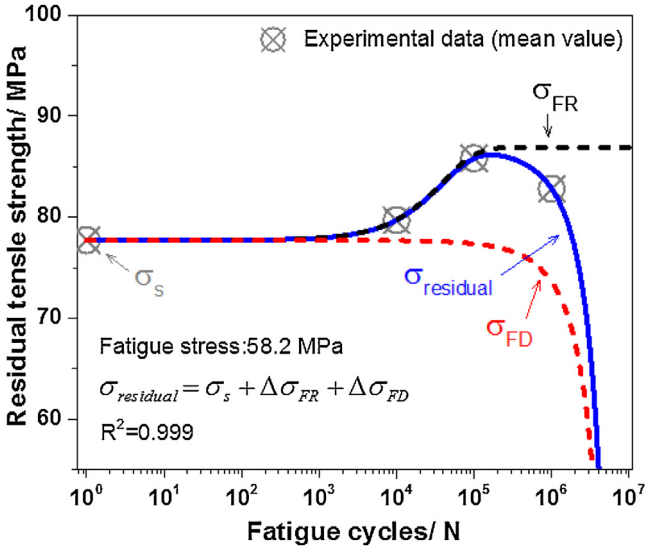


**Fig. 9.** The evolution of $\Delta\sigma_{FR}$, $\Delta\sigma_{FD}$ and $\sigma_{residual}$ as a function of the applied fatigue cycles for a fatigue stress of 58.2 MPa.

Based on the experimental results, Eqs. (1–3) can be then analyzed with a nonlinear algorithm. The best fitting curve of the RTS for a fatigue stress of 58.2 MPa is shown by the blue solid line in Fig. 9, together with the development of $\sigma_{FR}$ and $\sigma_{FD}$. Additionally, the used parameters for Eqs. (1–3) are listed in Table 4.

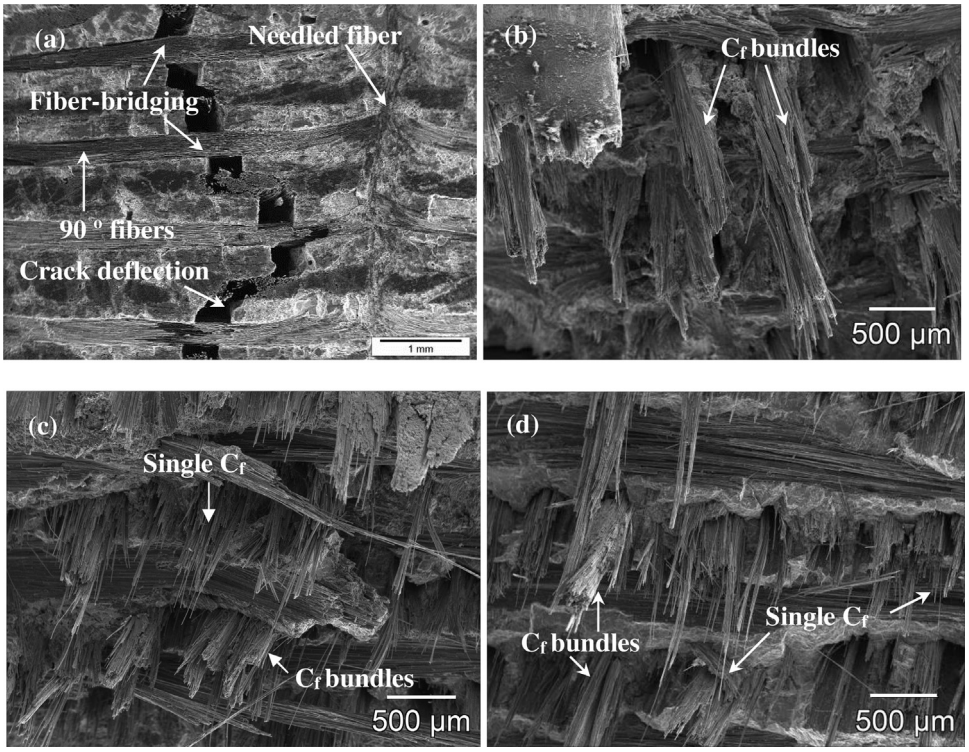


**Fig. 8.** The SEM micrographs of fractured morphology of the 2.5D C/C-SiC composites after quasi-static tensile test. (a) Typical crack pattern within one fatigued sample after $10^6$ cycles; (b) The fractured surface of the virgin sample; (c) The fractured surface of the fatigue loaded sample after $10^5$ cycles with the stress level of 90% (69.9 MPa); (d) The fractured surface of the fatigue loaded sample after $10^6$ cycles with the stress level of 75%(58.2 MPa).

**Table 4**
The fitting parameters for Eqs. (1–3).

| Parameter | $N_{FR}$ | $N_{FD}$ | $\sigma_{max}$ | $\sigma_s$ | $c$ |
|---|---|---|---|---|---|
| Coefficients | $4.004 \times 10^4$ | $2.712 \times 10^6$ | 58.2 | 77.7 | 0.546 |

As shown in Fig. 9, the presented model can well estimate the RTS of 2.5D C/C-SiC composites after a fatigue loading. The fitting results indicate that the RTS of the 2.5D C/C-SiC composites increases slowly, and reaches the maximum value after around $10^5$ cycles. The RTS then sharply drops when the number of fatigue cycle exceeds $10^6$. In general, $\Delta\sigma_{FR}$ occurs in the initial fatigue cycles. As discussed in the above section, the increase of RTS is mainly caused by the relief of TRS and elimination of stress concentrations in the composites. $\Delta\sigma_{FD}$ occurs throughout the whole fatigue loading, and is mainly attributed to the collective effect of interfacial friction/wear, fiber wear, and fiber breakage, which is more pronounced after several fatigue cycles.

## 4. Conclusions

The fatigue behavior and the stress-dependence and cycles-dependence of residual tensile strength for a 2.5D C/C-SiC composite were studied. Experimentally, the residual strengths of the specimens after fatigue loading with preselected stresses and cycles were investigated. Additionally, a mechanical model was applied to estimate the residual tensile strength of 2.5D C/C-SiC composites versus the fatigue cycles on the basis of the experimental results. Based on the performed investigation, following conclusions could be drawn:

(a) The 2.5D C/C-SiC show an excellent fatigue resistance. The fatigue limit (run-out of $10^6$ cycles) for the 2.5D C/C-SiC composites is 58.2 MPa (corresponding to the stress level of 75%).
(b) The fatigue loading results in enhancement of the ultimate residual tensile strength in all case of fatigue loading. The RTS of the specimens loaded with stress levels of 75%, 80%, 85% and 90% for fatigue for $10^5$ cycles are approximately 85.8, 84.3, 86.6 and 92.5 MPa, respectively, which are quite higher than the original 2.5D C/C-SiC specimens (77.7 MPa).
(c) The multiplication of matrix crack decreases the stress concentration, relieves the thermal residual stresses in the 2.5D C/C-SiC composites and results in the strength enhancement. Additionally, the fatigue damage could lead to a reduction of elastic modulus and linear behavior in the quasi-static tensile test.
(d) The RTS is dependent on the applied fatigue cycles. When the 2.5D C/C-SiC specimens are subjected to the stress of 58.2 MPa, the maximum RTS of the 2.5D C/C-SiC is determined with 85.8 MPa after $10^5$ cycles. Then the RTS decrease to 82.8 MPa after $10^6$ fatigue loadings.
(e) The mechanical model which considers the collective effects of strength enhancement/degradation which are induced by fatigue stress is proven to evaluate the RTS of the 2.5 D C/C-SiC composite versus the number of applied fatigue cycles with accuracy.

## Acknowledgements

The project was supported by the Nonferrous Metal Oriented Advanced Structural Materials and Manufacturing Cooperative Innovation Center in Central South University and the National Natural Science Foundation of China (Grant No. 51575536), Natural Science Foundation of Hunan Province (Grant No. 2015JJ3163) and Science and Technology Planning Project of Hunan Province (Grant No. 2015RS4016). Additionally, the authors would like to express the heartfelt gratitude to Mr. A. Mainz in the Department of Polymer Engineering, Mr. W. Freudenberg and Mr. T. Liensdorf in the Ceramic Materials Engineering, University of Bayreuth for their kind help with mechanical tests, and to Dr. Jiang Shao-hua and Mr. Lu Yu-hai for linguistic assistances during the preparation of this manuscript.

## References

[1] R. Naslain, Design, preparation and properties of non-oxide CMCs for application in engines and nuclear reactors: an overview, Compos. Sci. Technol. 64 (2) (2004) 155–170.
[2] W. Krenkel, F. Berndt, C/C–SiC composites for space applications and advanced friction systems, Mater. Sci. Eng.: A 412 (1–2) (2005) 177–181.
[3] H. Abu El-Hija, W. Krenkel, S. Hugel, Development of C/C–SiC brake pads for high-performance elevators, Int. J. Appl. Ceram. Technol. 2 (2) (2005) 105–113.
[4] W. Krenkel, Carbon fiber reinforced CMC for high-performance structures, Int. J. Appl. Ceram. Technol. 1 (2) (2004) 188–200.
[5] W. Krenkel, J. Georges Thébault, Ceramic matrix composites for friction applications, in: Ceramic Matrix Composites, John Wiley & Sons Inc., 2014, pp. 647–671.
[6] P. Xiao, Z. Li, X. Xiong, Microstructure and tribological properties of 3D needle-punched C/C–SiC brake composites, Solid State Sci. 12 (4) (2010) 617–623.
[7] Z. Li, P. Xiao, B.-g. Zhang, Y. Li, Y.-h. Lu, S.-h. Zhu, Preparation and dynamometer tests of 3D needle-punched C/C-SiC composites for high-speed and heavy-duty brake systems, Int. J. Appl. Ceram. Technol. 13 (3) (2016) 423–433.
[8] Q. Shi, P. Xiao, Effect of pyrolytic carbon content on microstructure and tribological properties of C/C–SiC brake composites fabricated by isothermal chemical vapor infiltration, Solid State Sci. 14 (1) (2012) 26–34.
[9] Z. Li, P. Xiao, B.-g Zhang, Y. Li, Y.-h Lu, Preparation and tribological properties of C/C–SiC brake composites modified by in situ grown carbon nanofibers, Ceram. Int. 41 (9 (Part B)) (2015) 11733–11740.
[10] S. Fan, L. Zhang, L. Cheng, S. Yang, Microstructure and frictional properties of C/SiC brake materials with sandwich structure, Ceram. Int. 37 (7) (2011) 2829–2835.
[11] S. Fan, L. Zhang, L. Cheng, G. Tian, S. Yang, Effect of braking pressure and braking speed on the tribological properties of C/SiC aircraft brake materials, Compos. Sci. Technol. 70 (6) (2010) 959–965.
[12] S. Fan, L. Zhang, Y. Xu, L. Cheng, J. Lou, J. Zhang, L. Yu, Microstructure and properties of 3D needle-punched carbon/silicon carbide brake materials, Compos. Sci. Technol. 67 (11–12) (2007) 2390–2398.
[13] Y. Wang, H. Wu, Microstructure of friction surface developed on carbon fibre reinforced carbon–silicon carbide (Cf/C–SiC), J. Eur. Ceram. Soc. 32 (12) (2012) 3509–3519.
[14] Y. Wang, H. Wu, Friction surface evolution of carbon fibre reinforced carbon/silicon carbide (Cf/C-SiC) composites, J. Eur. Ceram. Soc. 30 (15) (2010) 3187–3201.
[15] A. Morales-Rodríguez, M. Moevus, P. Reynaud, G. Fantozzi, Strength enhancement of 2D-SiCf/SiC composites after static fatigue at room temperature, J. Eur. Ceram. Soc. 27 (11) (2007) 3301–3305.
[16] A.G. Evans, F.W. Zok, R.M. McMeeking, Fatigue of ceramic matrix composites, Acta Metall. Mater. 43 (3) (1995) 859–875.
[17] P. Reynaud, Cyclic fatigue of ceramic-matrix composites at ambient and elevated temperatures, Compos. Sci. Technol. 56 (7) (1996) 809–814.
[18] P. Reynaud, A. Dalmaz, C. Tallaron, D. Rouby, G. Fantozzi, Apparent stiffening of ceramic-matrix composites induced by cyclic fatigue, J. Eur. Ceram. Soc. 18 (13) (1998) 1827–1833.
[19] Y. Zhang, L. Cheng, L. Zhang, X. Luan, Comparative analysis of low-cycle fatigue behavior of 2D-Cf-PyC/SiC composites in different environments, Int. J. Appl. Ceram. Technol. 12 (3) (2015) 491–499.
[20] B.F. Sørensen, J.W. Holmes, E.L. Vanswijgenhoven, Rate of strength decrease of fiber-reinforced ceramic-matrix composites during fatigue, J. Am. Ceram. Soc. 83 (6) (2000) 1469–1475.
[21] M. Mizuno, S. Zhu, Y. Nagano, Y. Sakaida, Y. Kagawa, M. Watanabe, Cyclic-fatigue behavior of SiC/SiC composites at room and high temperatures, J. Am. Ceram. Soc. 79 (12) (1996) 3065–3077.
[22] H. Mei, L. Cheng, Stress-dependence and time-dependence of the post-fatigue tensile behavior of carbon fiber reinforced SiC matrix composites, Compos. Sci. Technol. 71 (11) (2011) 1404–1409.
[23] D. Koch, K. Tushtev, G. Grathwohl, Ceramic fiber composites: experimental analysis and modeling of mechanical properties, Compos. Sci. Technol. 68 (5) (2008) 1165–1172.

[24] Y. Li, P. Xiao, Z. Li, W. Zhou, T. Liensdorf, W. Freudenberg, N. Langhof, W. Krenkel, Tensile fatigue behavior of plain-weave reinforced Cf/C–SiC composites, Ceram. Int. 42 (6) (2016) 6850–6857.
[25] C. Liu, L. Cheng, X. Luan, B. Li, J. Zhou, Damage evolution and real-time non-destructive evaluation of 2D carbon-fiber/SiC-matrix composites under fatigue loading, Mater. Lett. 62 (24) (2008) 3922–3924.
[26] K. Reifsnider, W. Stinchcomb, T. O'Brien, Frequency effects on a stiffness-based fatigue failure criterion in flawed composite specimens, in: Fatigue of Filamentary Composite Materials, ASTM International, 1977.
[27] S. Sarkani, G. Michaelov, D.P. Kihl, D.L. Bonanni, Comparative study of nonlinear damage accumulation models in stochastic fatigue of FRP laminates, J. Struct. Eng. 127 (3) (2001) 314–322.
[28] G. Fang, X. Gao, S. Zhang, J. Xue, Y. Song, F. Wang, A residual strength model for the fatigue strengthening behavior of 2D needled CMCs, Int. J. Fatigue 80 (2015) 298–305.